Accepted Manuscript

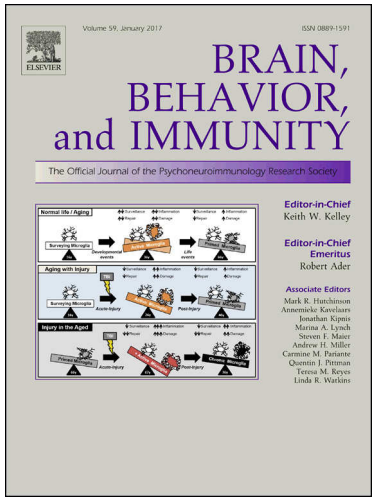

Brain grey matter volume reduction and anxiety-like behavior in lipopolysaccharide-induced chronic pulmonary inflammation rats: A structural MRI study with histological validation

Ji Chen, Ya Yan, Fengjuan Yuan, Jianbo Cao, Shanhua Li, Simon B. Eickhoff, Jiaxing Zhang

PII: S0889-1591(18)30858-4
DOI: https://doi.org/10.1016/j.bbi.2018.11.020
Reference: YBRBI 3539

To appear in: *Brain, Behavior, and Immunity*

Received Date: 28 March 2018
Revised Date: 1 October 2018
Accepted Date: 21 November 2018

Please cite this article as: Chen, J., Yan, Y., Yuan, F., Cao, J., Li, S., Eickhoff, S.B., Zhang, J., Brain grey matter volume reduction and anxiety-like behavior in lipopolysaccharide-induced chronic pulmonary inflammation rats: A structural MRI study with histological validation, *Brain, Behavior, and Immunity* (2018), doi: https://doi.org/10.1016/j.bbi.2018.11.020

Brain grey matter volume reduction and anxiety-like behavior in lipopolysaccharide-induced chronic pulmonary inflammation rats: A structural MRI study with histological validation

Ji Chen[1,2,3,*], Ya Yan[1], Fengjuan Yuan[1], Jianbo Cao[4,5,6], Shanhua Li[1], Simon B. Eickhoff[2,3], Jiaxing Zhang[1,*]

[1]Institute of Brain Diseases and Cognition, Medical College of Xiamen University, Xiamen, China
[2] Institute of Neuroscience and Medicine, Brain and Behaviour(INM-7), Research Centre Jülich, Jülich, Germany;
[3] Institute of Systems Neuroscience, Medical Faculty, Heinrich Heine University Düsseldorf, Düsseldorf, Germany;
[4]State Key Laboratory of Molecular Vaccinology and Molecular Diagnostics Center for Molecular Imaging and Translational Medicine, School of Public Health, Xiamen University, Xiamen, China.
[5] Medical College of Xiamen University, Xiamen, China
[6] Department of Radiology, University of Pennsylvania, Philadelphia, PA, USA

*_Corresponding authors_:

Prof. Jiaxing Zhang

Institute of Brain Diseases and Cognition, Medical College of Xiamen University, South Xiang'an Road, Xiamen, 361102, Fujian Province, China.E-mail: zhangjiaxing@xmu.edu.cn.

Ji Chen

Institute of Neuroscience and Medicine (INM-7, Brain and Behaviour), Research Centre Jülich, Jülich, 52428, Germany.E-mail: jichen.allen@hotmail.com.

Key words: chronic systemic inflammation, cytokines, voxel-based morphometry, brain MRI, histological validation

Abstract

While there have been multiple fMRI studies into the brain functional changes after acutely stimulated peripheral infection, knowledge for the effect of chronic peripheral infection on whole brain morphology is still quite limited. The present study was designed to investigate the brain structural and emotional changes after peripheral local infection initiated chronic systemic inflammation and the relationship between circulating inflammatory markers and brain grey matter. Specifically, *in-vivo* T2-weighted MRI was performed on rats with lipopolysaccharide (LPS)-induced chronic pulmonary inflammation (CPI) and those without. Grey matter volume was quantified using diffeomorphic anatomical registration through exponentiated lie (DARTEL) enhanced voxel-based morphometry followed by between-group comparison. Open field experiment was conducted to test the potential anxiety-like behaviors after CPI, along with the ELISA estimated inflammatory markers were correlated to grey matter volume. Guided by image findings, we undertook a focused histological investigation with immunefluorescence and Nissl staining. A widespread decrease of grey matter volume in CPI-model rats was revealed. 8 of the 12 measured inflammatory markers presented differential neuroanatomical correlation patterns with three of the pro-inflammatory cytokines (IL-1β, IL-6 and TNF-α) and CRP being the most notable. Lower grey matter volumes in some of the inflammatory markers related regions (amygdala, CA2 and cingulate cortex) were associated with more-severe anxiety-like behaviors. Furthermore, grey matter volumes in amygdala and CA3 were correlated negatively with the expressions of glial proteins (S100β and Nogo-A), while the grey matter volume in hypo-thalamus was changing positively with neural cell area. Overall, the neuroanatomical association patterns and the histopathology underpinning the MRI observations we demonstrated here would probably serve as one explanation for the cerebral and emotional deficits presented in the patients with CPI, which would furthermore yield new insights into the adverse effects the many other systemic inflammation and inflammatory autoimmune diseases would pose on brain morphology.

Introduction

Accumulated evidence shows that peripheral inflammation can affect the central neural system (CNS) via multiple pathways, including fast neural (autonomic nervous system), as well as slow humoral [cytokine and hypothalamic-pituitary-adrenal axis (HPA)] mechanisms (Konsman et al., 2002; Dantzer et al., 2008). In the humoral mechanism, the elevated circulating cytokines serve as the major mediators that activate the HPA, thus causing fever (Parsadaniantzet al., 2000; Rivest, 2001), and can act on the brain directly through 1) volume transmission from the choroid plexus into the surrounding brain parenchyma (Banks et al., 2002); 2) passive diffusion through circumventricular organs (Rivest, 2001) and 3) BBB leakage following disruption by specific inflammatory cytokines (Banks, 2005; Banks et al., 2015). Also, cytokines can target the afferents of the autonomic nerves that innervate the site of infection, contributing to the involvement of the neural mechanisms. Notably, the vagus nerve innervates most of the internal organs including the lungs and gastrointestinal tract, which can express cytokine receptors (Ek et al., 1998) and be stimulated by locally produced cytokines, thus sending inflammatory signals to the primitive areas of the brain (e.g., the nucleus tractus solitarius and lateral medulla; Dantzer et al., 2007). The activated vagus nerve could further influence the activation of the parabrachial nucleus and limbic regions through its projections (Dantzer et al., 2008). During the innate immune response phase, inflammatory cytokines play a pivotal role in bringing peripheral inflammatory signals to the brain (Capuron and Miller, 2004). As a non-invasive, high-resolution mapping technique, magnetic resonance imaging (MRI) is promising and has already contributed to the understanding of the brain-immune communication. A substantial proportion of previous MRI studies conducted on human samples have focused on brain functional responses to acutely stimulated peripheral infections (Brydonet al., 2008, Harrison et al., 2009; Eisenberger et al., 2010). Only a few extant studies have investigated morphometric changes in the brain grey matter in some human chronic infectious disease, such as inflammatory bowel disease (Zikou et al., 2014) and Hepatitis C (Hjerrild et al., 2016). However, these studies failed to demonstrate a link between potentially enhanced inflammatory markers and brain structural deficits. Additionally, the between-group comparison results varied prominently. Further, the majority of animal MRI studies focused on the structural and functional changes in the brain following

central inflammation (Tambalo et al., 2015; Guevara et al., 2017), while only a few studies investigated chronic peripheral infection. Consequently, our knowledge regarding the chronic effect of systemic inflammation on brain structure, as well as the relationship between circulating inflammatory markers and brain grey matter volumes is still quite limited. Although several Inflammatory markers, including tumour necrosis factor alpha (TNF-α), C-reactive protein (CRP), and Interleukin-6 (IL-6) have been associated with brain grey matter volume reductions in the hippocampus and several other cortical regions in healthy middle-aged adults (Marsland et al., 2008; Marsland et al., 2015), the elderly population not affected by dementia (Zhang et al., 2016a; Gu et al., 2017) and chemotherapy-treated breast cancer survivors (Kesler et al., 2013), these studies presented inconsistent results and the demonstration of causal directions in the observed associations was inconclusive. Moreover, apart from CRP and some pro-inflammatory cytokines (IL-1β, IL-6 and TNF-α), other Inflammation-related factors such as anti-inflammatory cytokines, chemokines and relevant proteases may also exert negative effects on brain grey matter but very few studies exist to support the findings (Zhang et al., 2016a). A comprehensive profile of inflammatory marker-neuroanatomical relationships under chronic peripheral-initiated systemic inflammation remains unclear.

In the present study, we built an lipopolysaccharide (LPS)-induced chronic pulmonary inflammation (CPI) rat model to investigate the contribution of the circulating inflammatory markers to the structural abnormalities in the brain during chronic systemic inflammation. LPS is a potent stimulant of cytokine release which has been widely used to simulate infection-induced systemic inflammatory response in animal studies. Injecting LPS directly into the trachea could cause a series of pathological changes in the lungs and result in sustained pulmonary inflammation (Stolk et al., 1992; Vernooy et al., 2002). With the progression of pulmonary inflammation, the increased amount of cytokines released within the lungs and the bronchia spill into the circulatory system, promoting systemic inflammation. The elevated circulating cytokines may cause damage to many tissues and organs outside the lungs, including the brain (Barnes, 2010). Moreover, based on the previous studies demonstrating a substantial involvement of cytokines in mediating negative emotions by relaying peripheral inflammation message to the brain (Reichenberg et al., 2001; Wright et al., 2005), we performed a classic open field experiment as a reflection of the potential anxiety-like behaviours in CPI-model rats, to explore

the relationship between enhanced circulating Inflammatory markers and the emotional problems after CPI. Since brain structural deficits, such as grey matter volume reduction, as well as emotional deficits including depression and anxiety have been reported in patients with CPI (von Leupoldt et al., 2011; Zhang et al., 2013; Chen et al., 2016), modelling systemic inflammation by LPS-induced CPI is clinically informative. Further, apart from elucidating the contribution of the sustained inflammatory response and elevated inflammatory marker levels to the brain grey matter volume reduction, depression, and anxiety (Hynninen et al., 2005; Katon et al., 2007) prevalent in CPI patients, the model may also yield general implications for several other diseases involving systemic inflammation.

Voxel-based morphometry (VBM) was employed to derive grey matter volume measurements in the present study since it is well-established for structural brain quantification, independent of the inter-operator bias, and is neurobiologically relevant (Ashburner and Friston, 2000; Biedermann et al., 2016). Although VBM is sensitive enough to identify abnormal regions in the whole brain, it is difficult to elucidate the biological substrates of the VBM derivatives, since the MRI parameter of grey matter volume is a combination of various cellular events, and changes in the grey matter may also represent vascular changes (May and Gaser, 2006; Zatorre et al., 2012). Therefore, we also performed several targeted histological analyses to verify the MRI findings.

Overall, in the present study, we investigated an LPS-induced CPI rat model and utilized structural MRI quantification, behavioural assessment and histological analysis, to elucidate the effects of various circulating inflammatory markers on brain morphology after chronic peripheral inflammation. We hypothesized that the grey matter volume reductions can be observed in the CPI-model rats and these aberrant MRI findings can be explained by the elevated levels of circulating inflammatory markers, implicated as a neuroanatomical substrate of the potential anxiety-like behaviours in CPI-model rats, and further validated by histological measurements.

Materials and Methods

Rat model

45 8-week-old SPF (specific pathogen free) male Sprague-Dawley rats with body weights ranging from 330-380g were purchased from the experimental animal center of Xiamen University, China.

The protocols were approved by the Committee on Animal Care and Use at Xiamen University. These rats were randomly divided into two groups. All efforts were made to minimize animal suffering. All rats were maintained with a 12:12 hr light/dark cycle (lights on 07:00–19:00 hr) at 22 ±1℃ and had free access to food and water. 25 rats were set as controls and 20 rats were treated with trachea injection of LPS to develop a CPI model. In detail, the rats in the CPI-model group were firstly anesthetized by intraperitoneal injection of 3.5% chloral hydrate (10ml/kg), and were then fastened to a board with supine position, exposing the glottis. Saline solution dissolved LPS [200ul (1mg/ml); sigma L2880, 055:B5] was injected into the trachea by intravenous needle, and after which the board was rotated to ensure that the LPS was distributed uniformly within the lung. LPS was injected in the experimental group once a week for 8 consecutive weeks (a total of 8 times). In the control group, same volume of endotoxin free saline was injected into the tracheas of the rats instead of LPS. All of the following assessments were performed after 4 months. Pulmonary functions including forced expiratory volume at 50 and 100 milliseconds/forced vital capacity (FEV50/FVC, and FEV100/FVC), functional residual capacity (FRC) and chord compliance (Cchord) were measured using small animal spirometer (FinePointe™ NAM system, Buxco, USA) as previously described (Miklos et al, 2008).

MRI data acquisition

All the rats experienced MRI scanning in the Center for Molecular Imaging and Translational Medicine of Xiamen University on a Bruker BioSpec 9.4T small animal MRI scanner (94/20 USR, Bruker, Germany). Rats were anesthetized by passively inhaling isoflurane (3% for initial anesthesia, and 1.5-2% to maintain the narcosis) and were placed in a 40mm ID quadrature birdcage transceiver coil (Bruker, Germany). Physiological parameters of heart rate and breathing were monitored during the data acquisition process. High-resolution structural images were acquired for each rat by using a 3-dimensional T2-weighted magnetization-prepared rapid acquisition of a gradient echo sequence (MPRARE) with the following parameters: RARE factor=8, repetition time/echo time = 3500ms/36ms, field of view (FOV) = 3.84 × 3.84 cm^2, acquisition matrix = 384 × 384, slice thickness = 1.0 mm, 28 slices with no gaps.

Behavior assessment

According to previous literature, inflammation will induce various emotional problems, such as decreased motivation, anxiety and depression (Reichenberg et al., 2001; Wright et al., 2005). Here, we performed a classical open field test to detect the potential emotional changes (anxiety) in the CPI-model rats. Open field activity has been long taken as an indicator of rodent emotional state for several decades (Walsh and Cummins, 1976), and has been commonly used in previous studies to test the anxiety affective condition (e.g., Crumeyrolle-Arias et al., 2014).Testing was carried out in a square white plexiglas open field of 0.60m in each side, surrounded by four 50 cm high walls. The bottom of the apparatus was divided into 9 squares (20 × 20cm) for assessing locomotion. The central square was regarded as the "center" of the field. The test started by placing the rat in the center of the field, each rat was put in the central square one by one. The activities of each rat within 5 minutes were video-tracked and five measurements were recorded: 1). number of center entries during the 5 min test; 2). crossing counts (the number of squares crossed with the four paws); 3). number of defecation; 4). number of grooming; and 5). number of rearing. The field was cleaned with 70% ethanol thoroughly between tests. The "emotional" rats, as in the CPI modeling group, would respond passively to the novel environment with also limited activity. They avoid the center of the field, and show high defecation, low levels of grooming and rearing. These abnormal activities in the open-field test are usually adopted as a reflection of a high level of anxiety (Prut and Belzung, 2003).

Inflammatory markers

Enzyme-linked immunosorbent assay (ELISA) was used to determine the concentrations of inflammatory markers. 12 inflammatory markers were quantified to provide a comprehensive panel of inflammatory markers and their associations with brain structural abnormalities. Besides CRP and matrix metalloproteinase-9 (MMP-9), these measured inflammatory markers could be roughly classified into several subgroups functionally according to their major activities (Opal and DePalo, 2000; Dinarello, 2000), namely the pro-inflammatory [IL-1β, IL-6, TNF-α, interferon-γ (IFN-γ), and granulocyte-macrophage colony stimulating factor (GM-CSF)] cytokines, anti-inflammatory [IL-10 and transforming growth factor-β (TGF-β)] cytokines, and chemokines [IL-8, chemokine ligand 2 (CXCL2), and Clara cell secretory protein (CC16)], although they could behave both as a pro- and as an anti-inflammatory cytokines under different biological events

(Cavaillon, 2001). HIF-1α, an intermediate in both of innate immune response and hypoxia (Rius et al., 2008), was also measured. To quantify these markers, rats were rapidly decapitated after MRI scans and blood was immediately collected. Blood samples were then centrifuged at 7,000rpm for 10 minutes and the plasma was frozen at -80℃. Plasma levels of the inflammatory markers were measured using commercial ELISA kits (Neobioscience Technology Company, Shenzhen, China) following the manufacturers' protocols. Selection of inflammatory markers was due to their heavy involvements in LPS-induced inflammatory response and the pathological process of CPI.

MRI data processing

Automatic skull strip

The present study adopted an automatic template-based skull stripping method (Nie et al., 2012) to remove the non-brain tissues. This method has the advantages of high accuracy and efficiency (Nie et al, 2012). In brief, we created a rat brain template with extracranial tissues as the first step (Fig. 1B). Then, non-brain tissues were eliminated to derive the intracranial template. 1 and 0 were assigned to the intracranial template for binaryzation (1 for intracranial voxels and 0 for others, Fig. 1B) to form an intracranial mask image. Therefore, after normalizing each individual image to the with extracranial tissues rat brain template, one can use the deformation parameters to invert the intracranial mask back to each rat's native image space, and then the intracranial tissues could be conveniently extracted.

Before VBM was performed, we built a study-specific grey matter template to which all of the individual images can register and then can compare across different rats. The whole processes included three steps (Fig. 1B):

1). intensity-based tissue segmentation;

2). unified segmentation with tissue probability templates;

3). DARTEL-based template refinement and normalization.

Intensity-based tissue segmentation

The brain-extracted T2 images were first bias corrected. Then, the resulting images were segmented into grey matter, white matter and cerebrospinal fluid (CSF) using FSL's (version 5.0; Analysis Group, FMRIB, Oxford, UK) FAST5 (Smith et al., 2004). Given the lack of a priori

information on the probability distribution of different tissue classes in the rat brain, we first used an intensity-based tissue classification kernel (Pham et al, 1999). To enhance the tissue differentiation and to achieve a more refined classification of the T2-weighted images of rodent brain as proposed by previous studies (Li et al., 2009), we set the kernel to divide the brain tissue into 5 sub-parts, including 2 components of cortical and Hipp grey matter, 2 white matter components consisting of cortical (corpus callosum and internal capsule) and pontine white matter, and one CSF component. After the segmentation process was done, we merged the 2 components of grey matter to constitute the final grey matter class, and the 2 white matter components were added to constitute the final white matter class. The initial grey matter, white matter and CSF tissue prior probability templates (P_0) were created on the basis of these intensity-segmented images by iteratively linear and non-linear registrations, which were then served as the reference maps for the following unified segmentation.

Unified segmentation

Because intensity-based segmentation is sensitive to noise and the segmentation results are usually in poor classification accuracy, we employed a unified segmentation scheme afterwards to segment the individual rat brains for a second time using Statistical Parametric Mapping software (SPM8;www.fil.ion.ucl.ac.uk/spm). The unified segmentation program in SPM builds upon specific tissue probability templates (here the P_0 maps which derived from the intensity-based segmentation were used), allowing the propagation of additional structural information to each individual brain in the light of tissue priori probability templates and finally give rise to an improved classification accuracy. Since the segmentation algorithm in SPM is optimized for human brain, parameters for the segmentation, as well as the below DARTEL programs were adjusted to accommodate the rat brain data. During the unified segmentation, the program first normalized the whole rat brains to the P_0 maps non-linearly, and then it utilized a Gaussian mixture model to cluster the tissues according to signal intensities. Finally, the clustering results were combined with the tissue classes' information embedded in the P_0 maps using Bayes rule to form a new set of tissue probability maps (Ashburner and Friston, 2005). After the segmentation process, three tissue probability images of grey matter, white matter and CSF in native space for each rat brain were obtained.

DARTEL-based template refinement and VBM analysis

Lastly, we employed the diffeomorphic anatomical registration through exponentiated lie (DARTEL) technique to form the final tissue probability templates based on the unified segmented images. DARTEL (Ashburner, 2007) is a framework that was intended to achieve more accurate alignment among the brains of different subjects. Specifically, the tissue probability images of grey matter, white matter and CSF (in native space) for each rat brain were imported into the DARTEL toolbox (i.e. the DARTEL create template program) in SPM8. The whole process of DARTEL consists of 6 rounds and 18 in total iterations, generating 6 sets of tissue probability templates and flow field files for each rat brain. The grey matter, white matter and CSF templates generated in the last round of iteration were adopted as the final study-specific tissue probability templates (P_1), and the flow field images were used to normalize each rat brain's grey matter, white matter and CSF classes to the template space (P_1) with each voxel resampled to isotropic 0.1mm.

In order to derive between-group differences in grey matter volume, the normalized rat brain's grey matter, white matter and CSF classes were modulated to restore the volumetric information that lost during the high-dimensional spatial registration (i.e., preserve amount).The modulated grey matter images were then smoothed with an isotropic Gaussian kernel with a sigma of 0.7 mm. Total volume of each tissue type was extracted from the modulated images. Intracranical volume was calculated by adding up the grey matter, white matter and CSF volumes, and was controlled in global measurements and VBM analysis as a scaling factor. A flow chart (Fig. 1B) was presented to illustrate the whole structural MRI processes.

To reference our VBM results, we normalized the DARTEL-derived grey matter template (P_1) to the publically available Sprague-Dawley rat brain MRI atlas (Papp et al., 2014), and the normalization parameters were applied to the VBM results bringing them to the rat MRI atlas space.

Complementary MRI analysis

Since significant correlations between Inflammatory markers and brain grey matter volumes have been reported in healthy population by previous studies (Zhang et al., 2016a; Gu et al., 2017), in the main general linear model (GLM) analyses we combined both of the two groups to achieve a general association pattern. On the other hand, given the consideration that the correlation patterns in control rats and the CPI-model rats may be different, we performed an

additional GLM analysis to explore whether there is a group-by-IM interaction effect (i.e. whether the slopes of the inflammatory markers regressed on brain grey matter volume are significantly differed between the two groups).

HIF-1α has been shown to participate in BBB disruption (Higashida et al., 2011) and innate immune response (Rius et al., 2008), which may exert either a neuroprotective effect or mediate a neurotoxic effect depending on different biological processes (Yeh et al, 2011; Khan et al., 2017). Also, HIF-1α, together with pulmonary function levels could indirectly indicate the possible hypoxic conditions in CPI-model rats to some extent. To elucidate the impact of HIF-1α on brain grey matter volume and to test the possible contribution of hypoxia to brain grey matter volume reductions, we furthermore conducted two additional MRI analyses as follows: 1). the between group comparison of voxel-based grey matter volume was repeated after added HIF-1α and pulmonary function measures as covariances of no interest; 2). individual GLM analysis was performed with HIF-1α or a pulmonary function metric in the right hand regressing on the voxel-based grey matter volume to elucidate whether there is a significant correlation between them.

Histological analysis

Immunofluorescence staining

After MRI scanning and behavior testing, all of the rats were sacrificed and the brains were retained for histological analysis to validate the MRI findings. The isolated brains were immediately frozen in liquid nitrogen, and stored at 80℃. In consultation with the Paxinos' rat brain atlas in stereotoxic coordinates, 20μm thick sections of brain were cut with a cryostat microtome (HM 505-E, Germany), and the histological slices were carefully co-located with the MRI slices based on anatomical features present in both. Guided by MRI observations, five regions-of-interest (ROIs) of hippocampus (CA3), amygdala, hypothalamus (Hypo-Thal), insula and retrosplenial cortex (RS) covering both of the cortex and limbic regions in one characteristic slice (bregma: -3.2mm) for each rat were selected on which the following histological analyses were performed to verify the voxel-based grey matter volume decrease in CPI-model rats. To reduce bias, two adjacent sections of the characteristic slice were also analyzed. After 4% paraformaldehyde fixed for 10 min, sections were incubated with S100 calcium-binding protein β

(S100β) antibody (1:500 dilution, rabbit monoclonal, Abcam) and Nogo-A antibody (1:83 dilution, mouse monoclonal, BD Biosciences) in PBST containing 0.3% Triton X-100 overnight at 4℃, respectively. Then sections were incubated with 10% BSA for 20min. Subsequently, sections were incubated with biotinylated donkey anti-rabbit immunoglobulin G (IgG) (Santa Cruz Biotechnology, Inc. 1:100 dilution) and donkey anti-mouse immunoglobulin G (IgG) (Santa Cruz Biotechnology, Inc. 1:100 dilution), respectively, for 2h at room temperature. Finally, sections were covered with glycerol and positive cells were observed using Olympus microscope.

Nissl staining

Brain slices (20μm) were mounted on targeting molecule polysine-coated slides and stained with 0.5% fast cresyl violet (LAICA, Bensheim, Germany) for 20 min at room temperature. Then brain slices were progressively dehydrated in alcohol, cleared in xylene, and covered with neutral balsam and coverslips.

Five frames of the immunofluorescence and Nissl staining images covering the above mentioned 5 ROIs were semi-quantitatively analyzed using ImageJ software (NIH). The fluorescence intensity per area (FIPA) index was calculated as IntDen/Area (where IntDen is the fluorescent cells integrated density in the image and Area is the region of fluorescence in the image). The relative cell area index, which derived from the Nissl staining maps by dividing the selected cell area within a frame by the total area of the whole frame, was used as a reflection of histological changes of neuronal cells.

Statistical analysis

The all measured inflammatory markers were correlated to each other to explore their association patterns using Pearson correlation analysis in SPSS, Version 19.0 (IBM, NY, USA). This correlation analysis was done separately for the control group and the CPI-model group since the interplay between each of the inflammatory marker pair may be differed in normal and diseased conditions. Between-group differences in intracranical volume, total volume of each tissue type, inflammatory markers and behavior metrics were also evaluated in SPSS. Parametric and nonparametric tests were used where appropriate depending on the distribution of the data. One-sample Kolmogorov-Smirnov test was used to evaluate the data normality. To test whether there is a significant difference in any of the inflammatory markers between the two groups, we

first constructed a mixed-model designed ANOVA analysis to examine the effect of inflammatory marker by group interaction. The all inflammatory markers were entered as within-subject variables and the group (control VS. CPI-model) was entered as a between-subject effect. Threshold was set at $p < 0.05$. Follow-up two-sample t-tests were performed when the inflammatory marker by group interaction was significant, checking exactly which of the Inflammatory markers were significantly differed between the two groups. Results of the post-hoc analysis were corrected for multiple comparisons via Bonferroni method ($p < 0.0038$). According to the Kolmogorov-Smirnov test, two sample Mann-Whitney *U* test was used for the two behavior metrics of number of defecation and number of center entries. For the other three behavior metrics, two sample t-tests were used. A Bonferroni correction was also applied with a cutting point of $p = 0.01$.

For VBM, a two-sample t-test was conducted in SPM8 to test voxel-based grey matter volume differences between the two groups. Head size was controlled by adding intracranical volume as a covariate of no interest. The statistical map was corrected for multiple comparisons across voxels through non-parametric testing with the Threshold-Free Cluster Enhancement (TFCE) technique by an extension toolbox of SPM, i.e. the TFCE toolbox (version 119, http://dbm.neuro.uni-jena.de/tfce). Statistical threshold was first set at Family-Wise Error (FWE) corrected $p < 0.05$ after 5000 permutations; a more conservative threshold of FWE corrected $p < 0.01$ was also applied to expect a more localized pattern. Subsequently, we constructed a single GLM for each inflammatory marker in SPM8 to test the general correlation pattern between the concentration of each inflammatory marker and the voxel-based grey matter volume in the combined group. Moreover, we constructed a joint GLM with all of the inflammatory markers as predictors to explore whether there is a specific effect of each IM on the brain grey matter volume given that the inflammatory markers may correlate to each other. The problem of multiple comparisons was addressed by the same correction method (TFCE) mentioned above with a threshold of FWE corrected $p < 0.05$.

ROI based correlation analysis was conducted to complement the whole brain voxel-wise correlation analysis since neuroanatomical correlations of some inflammatory markers and behavior measurements (especially, which only 23 rats in the control group and 13 rats in the CPI-model group were available) may not significant after applied a conservative correction

strategy of TFCE across the massive voxels of the entire brain. ROIs were selected based on the significantly between-group differed anatomical regions and were defined by masking the whole significant clusters by the brain parcels taken from the Waxholm MRI atlas. Since the latest version of the Waxholm MRI atlas does not encompass a full parcellation of the brain regions, those between-group differed anatomical regions that have not been outlined in the Waxholm MRI atlas were represented by spheres with 0.4mm radius after consulted the Paxinos' stereotactic atlas (Paxinos and Watson, 2014). After the ROIs were defined, mean grey matter volumes within the ROIs were extracted. Then, the extracted grey matter volumes were corrected for head size. Here, we adopted a regression-based correction approach to adjust the raw grey matter volumes (Chen et al., 2017). This method adjusts the observed volumes by an amount proportional to the difference between an individual's observed intracranical volume and the mean intracranical volume for all subjects, which has been presented as an accurate and reliable correction method (Jack et al., 1989). The equation is given as follows:

$$Volume(adjusted) = volume(observed) - B(ICV_i - ICVmean)$$

where ICV_i = the ith subject's intracranical volume, ICV_{mean} = overall average intracranical volume, and B is the slope of the regression line of each deep grey matter structure, regressed on intracranical volume. After head-size correction, Pearson or Spearman rank correlation analysis was performed where appropriate.

For histological measures, the averaged values (FIPA and relative cell area) of the three analyzed sections for each rat were obtained which were then compared between the two group using two sample t-tests, and were correlated to MRI measurements, behavior metrics and inflammatory markers in SPSS using Pearson correlation analysis or Spearman rank-correlation where appropriate. FDR correction was followed to control for type 1 error as there are multiple correlations conducted, and the FDR corrected q values were reported in additional to the original p values for those correlations survived in the multiple comparison corrections. Since there are 12 inflammatory markers involved and some of them were more closely related than the others (Zhang et al., 2016), we further employed the well-established principal component

analysis (PCA) with Varimax rotation to aggregate the 12 inflammatory markers into subsets to alleviate multiple comparisons and strengthen the findings. Before PCA was conducted, the 12 variables were fisher z-transformed over the rats to adjust the different scaling between the inflammatory markers. After the components (i.e., composite markers; CM) were identified, a rank-transformation was performed on the inflammatory markers for each rat, and each CM was formed as the averaged ranking over its component IMs per rat (a higher ranking refers to a more-severe inflammatory response). Afterwards, we correlated the resulted CMs to the histological measures using Spearman rank correlation in SPSS. Besides the above demonstrated correlation analyses, we finally performed a mediation analysis to estimate and test the possible mediators of histological metrics in the association between the experimental condition (CPI) and the outcome measurement of grey matter volume changes. To carry out the mediation analysis, we followed the PROCESS (http://www.process macro.org/) procedure for SPSS which based on ordinary least squares path analysis of regression (Hayes, 2018). As shown in the diagram (supplementary figure. 3), the a-path tests the experimental effect on the possible mediator, while the b-bath tests for the effect of mediator in predicting the outcome variable (here changes in grey matter volume) after controlling for the direct effect (c') of CPI on the outcome variable. In this context, a*b gives the mediation effect representing the indirect effect of causal condition on the outcome variable through possible mediators (here the histological changes), while inference of the indirect effect was based on the confidence interval (CI) that estimated through percentile bootstrapping approach. Specifically, 10,000 bootstrap samples were drawn with replacement from the original sample, and the regression analysis as for testing the indirect effect was repeated in each of the bootstrapped samples. Of those analyses, if the 95% CI of the generated statistics does not across zero, indicating there is evidence of an indirect effect for a tested mediator (Hayes, 2018). Apart from the primary mediation model presented above, we conducted three complementary mediation analyses by substituting 1) the histological metrics for each of the 12 measured inflammatory markers; 2) the histological metrics for pulmonary function parameters; and 3) the grey matter volume for behavior measurements.

Results:

Basic physiological measures

No significant body weight difference was found between the two groups at the time of behavior testing and MRI scanning ($p > 0.05$). Pulmonary function testing (FinePointe™ NAM system, Buxco, USA) showed that FEV50/FVC was significantly lower in CPI-model rats ($p = 0.002$), while FRC was significantly increased in CPI-model rats when compared to the control group ($p < 0.001$). These results indicated that the pulmonary function in CPI-model rats was deteriorated. In contrast, there were no significant differences in Cchord and FEV100/FVC between the two groups ($p > 0.05$).

Between-group comparison and intercorrelation of the inflammatory markers

We found that, more than a half of our measured inflammatory markers were significantly increased in the CPI-model group. In detail, the Mauchly's sphericity test in the mixed-model ANOVA analysis was significant ($p < 0.001$), which indicated that the variances between our measured inflammatory markers are not equal. Therefore, a Greenhouse-Geisser correction was made and the corrected results were reported for the mixed-model ANOVA. With this mixed model, a significant inflammatory marker by group interaction was noticed ($p = 0.002$, partial eta squared = 0.163). Post-hoc two sample t-tests showed that the 7 inflammatory markers of IL-1β, IL-6, TNF-α, IL-8, CC16, MMP-9 and CRP were all significantly differed between the two groups after corrected for multiple comparisons with higher values in the CPI-model group (all $p < 0.001$). Although the between-group differences in the concentrations of CLCX-2, IFN-γ and IL-10 were not survived after Bonferroni correction, they were significant ($p < 0.05$) at uncorrected levels (Table.1). Intercorrelations between the inflammatory marker-pairs showed different patterns for the control and the CPI groups. Multiple significant correlations were noticed in the control group, which showed that each pair of the 4 pro-inflammatory cytokines (TNF-α, IL-1β, IL-6, and GM-CSF) was positively correlated. The significant correlations of HIF-1α with IL-1β, TNF-α, GM-CSF, TGF-β, IL-8, CRP, and MMP-9 were found, indicating a positive co-varying between the transcription of HIF-1α and the increases of some cytokines. In contrast, multiple correlation patterns were vanished or inverse in the CPI-model group, indicating a disturbed immune homeostasis. Detailed information for these correlations can be found in Fig. 2.

Behavior testing

Since the number of center entries ($p = 0.008$) and the number of defecation were not normally distributed ($p = 0.001$, one-sample Kolmogorov-Smirnov test), two-sample Mann-Whitney *U* test

was adopted for these two metrics comparing between the two groups. No significant between-group differences were detected for the number of defecation (U = 108.5, p = 0.244) and the number of center entries (U = 117.0, p = 0.146). Two sample t-tests (control - CPI) on the other three metrics of crossing counts (t = 2.387, p = 0.023), number of grooming (t = 2.794, p = 0.016) and number of rearing (t = 2.538, p = 0.008) showed that the values were all significantly higher in the control group than that in the CPI-model group (Table. 1).

MRI findings

Between-group comparison

Greenhouse-Geisser corrected results were reported for the global analysis due to p < 0.001 in the Mauchly's sphericity test. A significant global metric by group interaction was found (p < 0.001, partial eta squared = 0.235). Post-hoc analysis showed no significant between-group differences in total WM volume (p = 0.144) and intracranical volume (p = 0.356), while the total grey matter volume was significantly reduced (p < 0.001) and the CSF volume was significantly increased in the CPI-model rats (p < 0.001) (Table. 1).

From the whole brain VBM analysis, a widespread brain area showed significantly decreased grey matter volume in the CPI-model rats when compared to the control group at a threshold of FWE corrected p < 0.05 (Fig. 3). The decreases of grey matter volume in multiple brain regions were still survived at FWE corrected p < 0.01 (Fig. 3). These regions covered (para)limbic and neocortical areas, including the bilateral thalamus (Thal), Hypo-Thal, hippocampus (CA1, CA2, CA3, DG), amygdala, substantia nigra (SN), lateral globus pallidus (LGP), caudate putamen (CPu), lateral septal nucleus (LSI), insula, cingulate cortex (Cg), RS, motor (M1/M2) and somatosensory cortex (S1/S2), auditory cortex (AuC), visual cortex (VC), superior colliculus (SC), perirhinal cortex (PER), temporal association cortex (TeA), ectorhinal cortex (Ect) and entorhinal cortex (Ent). These reported anatomical brain regions were spatially identified in comparison to the Waxholm brain MRI volumetric atlas (version 2, which includes the subfield delineations of Hipp; Papp et al., 2014; Kjonigsen et al., 2015) in a slice by slice manner, and also with consultation of the Paxinos' stereotactic rat brain atlas (Paxinos and Watson, 2014) which has a more refined definition of anatomical regions, especially in the neocortex.

Whole brain voxel-wise Correlation analysis

After permutation testing with TFCE technique on the individual GLMs, 8 of the 12 measured inflammatory markers were found to negatively correlate with some brain regions in voxel-based grey matter volume at FWE corrected $p < 0.05$, including three pro-inflammatory cytokines of IL-1β, IL-6, TNF-α, one anti-inflammatory cytokine of IL-10, two chemokines of IL-8 and CC16, and other two inflammatory markers of MMP-9 and CRP (Fig. 4). Among these 8 inflammatory markers, the three pro-inflammatory cytokines, MMP-9 and CRP were more prominent in the correlations with brain grey matter volume not only in spatial distribution (more extensive) but also in statistical significance (stronger) than the others. In detail, the three pro-inflammatory cytokines showed widespread negative correlations with the voxel-based grey matter volumes mainly in Hipp, Thal, Hypo-Thal, CPu, SN, RS and Ins. Brain regions detected for MMP-9 and CRP were extensive as well (11 and 14 regions for MMP-9 and CRP, respectively). In contrast, confined brain regions were revealed for IL-10, CC16 andIL-8. Among the all Inflammatory markers correlated brain regions, Hypo-Thal, Hipp, RS and CPu were the most frequently involved which correlated to 7 of the 8 Inflammatory markers. Please refer to Fig. 4C for a more intuitive view of the whole brain regions these inflammatory markers were significantly associated to, as well as the correlation strength ***r*** (scatter plots for these significant correlations were shown in supplementary figure. 1). Moreover, seen from Fig. 4B, the inflammatory markers related brain regions were largely overlapped with the areas (within red outlines) that were detected as significantly decreased grey matter volumes in CPI-model rats. No significant neuroanatomical correlations were found for other measured inflammatory markers (FWE corrected $p > 0.05$). The joint GLM with all of the measured 12 inflammatory markers as predictors revealed no significant results (FWE corrected $p > 0.05$). No significant correlation was found between the voxel-based grey matter volume and any of the behavior metric.

ROI-based correlation analysis

Among the all 23 anatomical brain regions that were reported in the between-group comparison analysis, 14 can be taken from the Waxholm brain MRI atlas and the remaining 9 regions were defined as sphere ROIs according to the Paxinos' stereotactic rat brain atlas. ROI-based correlation analysis showed that grey matter volumes in multiple brain regions of LGP ($r = 0.331$, $p = 0.048$), CA2 ($r = 0.334$, $p = 0.046$), Cg ($r = 0.395$, $p = 0.017$) and amygdala ($r = 0.350$, $p = 0.036$) were significantly positively correlated with the number of rearing (Fig. 5). Grey matter volumes

in the regions of Cg (r = 0.339, p = 0.043) and S1 (r = 0.373, p = 0.025) were changing positively with crossing counts (Fig. 5). Grey matter volume in LGP was found to significantly correlate with the number of grooming (r = 0.411, p = 0.013) (Fig. 5). There were no significant correlations between the concentrations of GM-CSF, IFN-γ, TGF-β and CXCL2 and the grey matter volumes measured by ROI-based analysis

Complementary MRI analysis

No significant inflammatory marker by group interaction was observed for any of the inflammatory marker in correlation to the voxel-based brain grey matter volume. The results remained unchanged after controlling for HIF-α level and the two significantly between-group differed pulmonary function measures of FEV50/FVC and FRC in the between-group comparison of voxel-based grey matter volume (Fig. 7). No significant correlations were detected between the HIF-1α level, FEV50/FVC, FRC, and voxel-based grey matter volume.

Histological analysis

Targeted histological analysis (Fig. 6) revealed that the MRI marker of grey matter volume in two of the selected brain regions was significantly correlated to the fluorescence intensity. In detail, the FIPA of S100β was significantly negatively correlated to the mean grey matter volume within the CA3 ROI (r = -0.412, p = 0.017) (supplementary figure. 2A), and the FIPA of Nogo-A showed a significant negative correlation with the averaged grey matter volume in amygdala ROI (r = -0.620, p < 0.001; FDR corrected q = 0.006) (supplementary figure. 2B). Significant correlations were also detected between the increased FIPAs and the abnormal open field behaviors. For S100β, the FIPA in amygdala was significantly negatively correlated with the number of rearing (r = -0.362, p = 0.049), and the FIPA in RS also showed significant negative correlations with the number of rearing (r = -0.436, p = 0.019; FDR corrected q = 0.035), the number of grooming (r = -0.429, p = 0.018; FDR corrected q = 0.035) and the crossing counts (r = -0.421, p = 0.021; FDR corrected q = 0.035). For Nogo-A, the FIPA in amygdala and the number of rearing was negatively correlated (r = -0.372, p = 0.043), and a significant negative correlation was also noticed between the FIPA in Hypo-Thal and the crossing counts (r = -0.385, p= 0.036). Besides, the enhanced expressions of both the S100β and Nogo-A were found to change positively with the higher concentrations of multiple inflammatory markers. For S100β, the FIPA in amygdala was significantly positively correlated with the concentrations of IL-6 (r = 0.413, p = 0.029), and IL-8 (r

= 0.442, p = 0.019); the FIPA in insula was correlated with IL-6 (r = 0.418, p = 0.027); and the FIPA in CA3 was correlated with IL-10 (r = 0.429, p = 0.023). For Nogo-A, the FIPA in amygdala was significantly positively correlated with the concentrations of IL-1β (r = 0.486, p = 0.009; FDR corrected q = 0.018), IL-6 (r = 0.698, p < 0.001; FDR corrected q = 0.006), TNF-α (r = 0.587, p = 0.001; FDR corrected q = 0.006), MMP-9 (r = 0.510, p = 0.006; FDR corrected q = 0.018), and CRP (r = 0.489, p = 0.008; FDR corrected q = 0.018); the FIPA in Hypo-Thal was correlated with IL-6 (r = 0.436, p = 0.020); the FIPA in insula was correlated with IL-6 (r = 0.456, p = 0.015), TNF-α (r = 0.432, p = 0.022), and IL-8 (r = 0.414, p = 0.028); the FIPA in CA3 was correlated with IL-6 (r = 0.395, p = 0.037), TNF-α (r = 0.394, p = 0.038), and CC16 (r = 0.484, p = 0.009).

Nissl staining revealed extensively reduced neuronal density and abnormally morphology in all of the five measured brain regions in the CPI-model rats when compared with control rats (Fig. 6B). In Hypo-Thal, the relative cell area index was significantly correlated with the averaged grey matter volume (r = 0.484, p = 0.049) (supplementary figure. 2C). Also, the relative cell area in RS was found to correlate with the number of grooming (r = 0.548, p = 0.035). Moreover, the reduced neural cells within the 5 brain regions were all correlated to the concentrations of multiple inflammatory markers. In detail, the relative cell area in CA3 was significantly negatively correlated with the levels of IL-1β (r = -0.707, p = 0.005; FDR corrected q = 0.012), IL-6 (r = -0.549, p = 0.042), TNF-α (r = -0.715, p = 0.004; FDR corrected q = 0.012), IL-8 (r = -0.735, p = 0.003; FDR corrected q = 0.012), CLCX2 (r = -0.517, p = 0.033), CC16 (r = -0.706, p = 0.005; FDR corrected q = 0.012), MMP-9 (r = -0.862, p < 0.001; FDR corrected q = 0.0009) and CRP (r = -0.658, p = 0.011; FDR corrected q = 0.022). The relative cell area in amygdala showed negative correlations with IL-6 (r = -0.564, p = 0.036) and TNF-α (r = -0.547, p =0.043). The relative cell area in insula was changing negatively with the levels of TNF-α (r = -0.676, p = 0.008; FDR corrected q = 0.032), IL-8 (r = - 0.648, p = 0.012; FDR corrected q = 0.036), CC16 (r = -0.768, p = 0.001; FDR corrected q = 0.012) and MMP-9 (r = -0.674, p = 0.008; FDR corrected q = 0.032). Significant negative correlations were also observed between the relative cell area in RS and IFN-γ (r = -0.594, p = 0.025) and CC16 (r = -0.606, p = 0.022). In addition, inflammatory markers of IL-6 (r = -0.576, p = 0.031), TNF-α (r = -0.593, p = 0.025), CC16 (r = -0. 795, p = 0.001; FDR corrected q = 0.12) and MMP-9 (r = -0.580, p = 0.030) were correlated negatively with the relative cell area in Hypo-Thal.

According to the Kaiser-Guttman rule, the first 2 components were retained which

explained 63.62% variance. Two separate CMs were identified with CM-1 consisting of TNF-α, IL-1β, IL-6, IL-8, INF-γ, CRP and MMP-9, CM-2 consisting of CC16, CXCL2, GM-CSF, TGF-β and IL-10. Except for the correlation between CM-1 and FIPA of Nogo-A in CA3 (*rho* = -0.410, p = 0.03), other detected significant correlations for CMs were all survived in FDR corrections (q < 0.05). Specifically, CM-1 was negatively correlated with the FIPA of Nogo-A in amygdala (*rho* = -0.468, q = 0.024), and insular cortex (*rho* =-0.530, q = 0.008), the FIPA of S100β in CA3 (*rho* =-0.476, q = 0.02), and were significantly positively correlated with the relative cell area in amygdala (*rho* = 0.675, q = 0.016), CA3 (*rho* = 0.776, q = 0.002), RS (*rho* =0.556, q = 0.043) and Hypo-Thal (*rho* = 0.771, q = 0.001). CM-2 were significantly negatively correlated with the FIPA of Nogo-A in insular cortex (*rho* =-0.384, q = 0.043), and were significantly positively correlated with the relative cell area in CA3 (*rho* = 0.556, q = 0.039), insular cortex (*rho* = 0.767, q = 0.024), RS (*rho* =0.547, q = 0.043) and Hypo-Thal (*rho* = 0.771, q = 0.001).

Mediation analysis

There was an evidence of indirect effect of CPI on grey matter volume reduction in the amygdala ROI through the increased expression of Nogo-A (higher in FIPA indicates more-severe neuronal injury). The 95% bootstrap CI for the mediation effect of Nogo-A using 10,000 bootstrap samples was entirely below zero (-0.0745 to -0.0021). No mediation effects were detected for other histological metrics and histologically analyzed ROIs. After substituting the histological metric for each of the 12 measured inflammatory markers in the mediation model, we found multiple indirect effects (all of the below mentioned CIs are 95% bootstrap CIs) of these elevated inflammatory markers in mediating the influence of CPI on regional brain grey matter volume reductions. Specifically, IL-6 mediated brain grey matter volume reductions in Cg (CI -0.0366 to -0.0004), CA2 (CI -0.0517 to -0.0001), and RS (CI -0.0616 to -0.0007); IL-1β mediated the decreased grey matter volumes in SC (CI -0.0521 to -0.0063) and Thal (CI -0.0459 to -0.0100); TNF-α mediated grey matter volume reductions in Thal (CI -0.0193 to -0.0002), CA3 (CI -0.0583 to -0.0085), CA2 (CI -0.0522 to -0.0001), LSI (CI -0.0448 to -0.0046), VC (CI -0.0415 to -0.0009), and SC (CI -0.0448 to -0.0021); IL-10 did have mediation effect on brain grey matter volume reductions in CA2 (CI -0.0401 to -0.0023), CA3 (CI -0.0306 to -0.0008), and M1 (CI -0.0332 to -0.0003); IL-8 mediated brain grey matter volume reductions in AuC (CI -0.0977 to -0.0026) and Ect (CI -0.0832 to -0.0009); MMP-9 mediated a decrease of brain grey matter volume in SN (CI -

0.0484 to -0.0005); C-reactive protein mediated the lower grey matter volumes in CA3 (CI -0.0375 to -0.0004), LSI (CI -0.0401 to -0.0001). In contrast, when substituting the histological metrics for pulmonary function parameters, we did not find any indirect effect (95% bootstrap CI passed zero) for each pulmonary function index in mediating CPI effect on the changes of brain grey matter volume. Lastly, by substituting the outcome variable of "changes in grey matter volume" for behavior metrics, we found that the CPI effect on the abnormal open field activities (decreased number of grooming in CPI-model rats) was mediated by an increased FIPA of S100β in RS (CI -1.484 to -0.006).

Discussion

In the present study, we investigated the effect of CPI on CNS via an LPS-induced CPI rat model, using voxel-based structural MRI quantification and histological analysis. Furthermore, neuroanatomical correlation patterns of various circulating inflammatory markers and neuroanatomical underpinnings of the CPI-induced anxiety-like behaviours were explored. The results showed that 1) CPI resulted in a widespread brain grey matter volume reduction **in** multiple (para)limbic and cortical brain areas; 2) out of the inflammatory markers measured, 8 presented differential, negative correlations with selective brain regions; 3) the brain regions associated with the inflammatory markers overlapped with those demonstrating the grey matter volume reduction, and some of them were associated with the anxiety-like behaviours observed in the CPI-rat model. 4) The MRI findings were validated by Nissl staining, as well as by measuring the levels of S100β and Nogo-A, the two proteins are considered as the biomarkers for brain injury. Histological metrics of FIPA and relative cell area were found to correlate with the abnormal behaviours and the elevated inflammatory markers.

MRI findings

LPS-induced CPI resulted in grey matter loss in several brain regions, which was in line with the previous human MRI studies revealing grey matter loss in the Hippcampus, Thal, Hypo-Thal, amygdala, insula, Cg, CPu, VC, occipitotemporal area and sensorimotor cortex (von Leupoldt et al., 2011; Zhang et al., 2013, Chen et al., 2016) in patients with sustained pulmonary inflammation, such as chronic obstructive pulmonary disease (COPD) and asthma. Similar regions, such as the CPu, Cg, Thal, occipitotemporal area and motor cortex were reported to be affected

in some chronic infectious diseases (Zikou et al., 2014; Hjerrild et al., 2016) and in patients with inflammatory autoimmune diseases, such as rheumatoid arthritis (Wartolowska et al., 2012) and systemic lupus erythematosus (Zhang et al., 2016b). Among these brain regions, hippcampus, SN, CPu, Cg, and insula have been associated with abnormally enhanced levels of pro-inflammatory cytokines (IL-6, IL-1β, TNF-α) in previous human fMRI studies (brain functional changes in response to acutely stimulated peripheral infection) (Brydon et al., 2008; Harrison et al., 2009). Further, although inconsistent, the associations between lower grey matter volume in hippocampus and higher levels of IL-6, TNF-α and CRP have frequently been reported in previous human studies (Marsland et al., 2008; Gu et al., 2017; Marsland et al., 2017), along with some other instances of occipitotemporal area, inferior parietal lobe and VC being mentioned (Zhang et al., 2016a). Here, we demonstrated a comprehensive neuroanatomical correlation pattern of various inflammatory markers after CPI, where the grey matter volumes in hippcampus, insula, Cg, SN, CPu, Thal, RS and VC correlated inversely with the levels of the measured inflammatory markers. These findings corroborated the previous reports of inflammatory markers-associated pathological changes in the aforementioned brain regions. Interestingly, the abnormally enhanced circulating inflammatory markers acted differentially on the structural abnormalities in selective brain regions, with three of the pro-inflammatory cytokines (IL-1β, IL-6 and TNF-α), MMP-9 and CRP being the most notable, while hippcampus, CPu and (Hypo-)Thal were the most prominently affected regions correlating to multiple inflammatory markers. The newly observed neuroanatomical correlation patterns could be explained possibly by the different roles the inflammatory markers played in the communication with the brain. For example, pro-inflammatory cytokines, such as IL-1β, IL-6 and TNF-α have been shown to act as mediators promoting neuroinflammation (Ramilo et al., 1990; Yang et al., 2013), leading to activation of glial cells (Semmler et al., 2005), decrease in the synaptic plasticity (Tancredi et al., 2000) and neuronal cell death (Vitkovic et al., 2000). In contrast, anti-inflammatory cytokines inhibit the production of pro-inflammatory cytokines and thus ameliorate brain damage. In addition, different brain regions may contain different kinds and amounts of inflammatory marker receptors. Nevertheless, the underlying mechanisms of the observed neuroanatomical correlation patterns and the reason why inflammatory markers differentially affect selective brain regions need to be further investigated.

Moreover, reduced grey matter volumes in the brain regions correlating with the levels of inflammatory markers—including amygdala, CA2, and Cg—also correlated with the measured anxiety-like behaviours [reduced exploration (number of rearing) and locomotor (crossing counts)] after CPI. Amygdala and Cg are known as important nodes in emotional processing and regulation (Pessoa, 2017), while CA2 has been proposed as a pivotal interface between the brain regions responsible for emotional processing and social memory (Chevaleyre et al., 2016). In line with our present results, previous human fMRI studies showed that the enhanced release of inflammatory markers after stimulated peripheral infection perturbed neuronal activations in reward circuit brain regions (such as amygdala), Cg and hippocampus, and these functional abnormalities mediated the observed neuropsychological deficits and mood changes, such as psychomotor slowing (Brydon et al., 2008) and anhedonia (Eisenberger et al., 2010). In addition, previous studies have also demonstrated that systemic administration of bacterial LPS, as well as the elevated inflammatory markers (such as IL-1β and IL-6) consistently suppress rodent locomotor and motivational activities and give rise to anxiety-like behaviours (Dantzer et al., 2007). Although previous researches have revealed a link between the levels of some inflammatory markers and grey matter volumes in hippocampus and Cg (Marsland et al., 2008; Marsland et al., 2015; Zhang et al., 2016a; Gu et al., 2017), these studies lacked relevant experiments to examine the potential emotional changes.

Complementary MRI analysis showed that the results of the between-group comparison in the voxel-based brain grey matter volume remained the same after adjusting for HIF-1α levels, and there was no significant correlation between HIF-1α and voxel-based grey matter volume. HIF-1α expression increases in hypoxic conditions, as the prolyl-hydroxylation of HIF-1α is prevented, which also plays an important role in innate immunity (Rius et al., 2008) and can be initiated by LPS and multiple inflammatory markers leading to HIF-1α accumulation (Frede et al., 2006). In the present study, we observed a non-significant increase in the HIF-1α in CPI-model rats. Depending on the biological conditions, HIF-1α can either exert a neuroprotective effect (Khan et al., 2017) or mediate a neurotoxic process resulting in neural cell death (Yeh et al., 2011). Our current findings indicated HIF-1α might tend to affect the brain structure through some indirect pathways, such as reinforcing the release of various inflammatory markers to promote neuroinflammation and/or mediate the production of neurotoxic factors following CPI.

Additionally, the absence of an association between brain structural deficits and pulmonary measures is in line with previous MRI studies in COPD (Dodd et al., 2012; Chen et al., 2016).

Histological correlates of the MRI findings, behavior metrics and inflammatory markers

Although the grey matter volumes derived using MRI can sensitively localize the abnormal brain regions, it still is a surrogate indicator of neuronal damage since the changes observed in grey matter volume can be a combination of many cellular processes, or even as a consequence of vascular changes (May and Gaser, 2006; Zatorre et al., 2012). These considerations limited the interpretation of many previous MRI studies to the links between inflammatory markers and the brain structural measurements. In the present study, we performed two targeted histological analyses, viz. immunofluorescence and Nissl staining, and found that higher expressions of S100β and Nogo-A correlated with lower grey matter volumes in the CA3 and amygdala, and a reduced cell area correlated with a grey matter volume reduction in the Hypo-Thal. Both Nogo-A and S100β are reported to increase after brain injury and could reflect the severity of neuronal damage (Rothermundtet al., 2003; Korfias et al., 2006). Furthermore, systemic inflammation and LPS stimulation lead to a profound glial activation (Semmleret al., 2005; Oyarzabal, 2016), while the cytokine production in the CNS and S100β can induce astrocyte activation, which in turn enhances the expression of glial proteins (Hunter et al., 1992; Hu et al., 1999;Lam et al., 2001). Here we also found that the level of S100β positively correlated with multiple circulating inflammatory markers, which corroborated the previous findings that the cytokines could up-regulate S100β expression following astrocyte activation. The cell area index derived from ImageJ is a combined reflection of neural cell size and density, while the qualitative analysis shown in Fig. 6 reveals that the neuronal cells are much sparser in CPI-model rats than in the controls. Corroborating with the previous literature (Raghavendraet al., 2004; Perry et al., 2007), neurodegeneration and glial activation may implicate the cellular pathology underpinning the brain deficits in systemic infections and inflammation. Moreover, in our study, some of the measured outcomes of the open field activity demonstrated a significant negative correlation with the S100β and Nogo-A expression in amygdala, RS and Hypo-Thal, and a positive correlation with the relative cell area in Hypo-Thal. This indicated that neurodegeneration and glial pathology may serve as the cellular mechanisms underpinning the anxiety-like behaviours

following CPI.

Mechanisms for the associations between inflammatory markers and brain structural deficits

Since the mechanisms by which peripheral inflammatory markers contribute to brain atrophy remain unclear, interpretations of our current findings can be manifold. First, circulating inflammatory markers could invade the CNS through several pathways, including active transport into the brain parenchyma (Banks et al., 2002), passive diffusion among circumventricular organs (Quan et al., 1998； Rivest, 2001) and particularly by unregulated leakage under the condition of BBB disruption following an inflammatory response (Banks, 2005; Banks et al., 2015). Multiple Inflammatory markers have been shown to play a role in BBB disruption, such as MMP-9, TNF-α, and HIF-1α measured in the present study (Kimet al., 1992; Higashida et al., 2011). The BBB breakdown largely facilitates the entry of other inflammatory markers into the CNS, establishing their direct communication with the immune and neural cells in the brain. The enhanced inflammatory marker levels, especially for the pro-inflammatory cytokines of IL-6, TNF-α and IL-1β could cause neurotoxicity through a possible β-amyloid pathway. Specifically, pro-inflammatory cytokines including IL-6 have been associated with an increased neuronal synthesis of β-amyloid directly in the brain (Jaeger et al., 2009). The enhanced neurotoxic amyloid peptide deposition induced by TNF-α and IL-1βhas been reported to contribute to neurodegenerative processes (Sastre et al., 2008). Also, the influx of peripheral pro-inflammatory cytokines could directly induce glial activation and neuronal cell death (Semmler et al., 2005). Moreover, there exists a cellular network within the brain which generates cytokines and expresses cytokine receptors (Dantzer et al., 2007). The abnormally enhanced inflammatory markers bind to the receptors in specific brain regions and promote neuroinflammation. For example, rodent studies showed an abundance of IL-6 receptors in the hippocampus, which can be activated by circulating inflammatory markers and then produce IL-6 (Gadient and Otten, 1994). The increased IL-6 concentration can ultimately be detrimental to the surrounding neural cells. Furthermore, we revealed that S100β and Nogo-A correlated positively with the grey matter volumes in several brain regions, which was in line with previous studies demonstrating that the expression of both the proteins increases proximal to the site of brain injury and is enriched

around the lesions (Rothermundt et al., 2003; Hunt et al., 2003; Shao et al., 2017). The over-expressed Nogo-A and S100β reinforce the inhibition of axonal recovery and structural remodelling and induce neuronal cell death on the top of the initial neuronal injury caused by the enhanced circulating inflammatory markers (Hu et al., 1997; Shao et al., 2017). Normal expression of S100β may enhance neural survival after tissue damage, but an abnormally high concentration of S100β may stimulate the production of pro-inflammatory cytokines, causing neurodegenerative effects (Rothermundt et al., 2003). This collectively indicated that controlling the expression of Nogo-A and S100β may help to alleviate a secondary injury following the initial insult by enhanced circulating inflammatory markers following sustained peripheral inflammatory response.

Limitations and strength

Firstly, apart from the open field test, several other tests could also reflect various aspects of the negative emotions following CPI, such as the sucrose preference test and the forced swim test. Nevertheless, the open field test is a classic test that can sensitively capture the changes in local activities and could reflect the anxiety levels in rodents under different experimental conditions (Prut and Belzung, 2003). Based on this test, we demonstrated an axis of the inflammatory-brain-behaviour relationship following CPI, which yielded new insights in this line of research. Secondly, the behavioural measurements and MR images obtained in the present study were cross-sectional and repeated measures of these metrics may help us to interpret the correlations between grey matter volumes and inflammatory markers during different phases of the CPI. Thirdly, beside the solid findings in whole brain voxel-wise analyses, for the other add-on analyses of relating brain grey matter volumes to behaviour and histological measurements, as well as the associations between inflammatory markers and specific histological metrics, yet exploratory, we still tried to balance the power of detecting significance while also controlling for type 1 error to strengthen the demonstration of the current findings as multiple variables were involved. As a solution, we reported both of the raw p-values and the FDR corrected q values for those survived after multiple comparison corrections. This motivation stemmed from the arguments that a combination of small sample sizes and stringent alpha-correction levels would lead to grossly inflated correlations (Yarkoni, 2009), but would benefit from a power analysis for

deciding optimal sample sizes in future studies. Moreover, we aggregated the 12 inflammatory markers into 2 subsets and demonstrated multiple significant correlations that survived a follow-up correction procedure with improved statistical justification. Further, the large MRI slice thickness reduced the scanning time but suffered the suboptimal matching with the histological sections. Nonetheless, we still did find some significant correlations between the MRI-derived grey matter volume and histological metrics (i.e. FIPA and relative cell area) in the analysed ROIs, which quite a few previous studies have addressed this kind of histological validation issue. Future studies based on the present, exploratory research, could focus on some specific brain regions and MRI slices (in rather high resolution, e.g., ~ 0.2 mm) to achieve a more precise spatial matching between the MRI measures and the histological analysis; allowing for more sophisticated and in-depth investigation of the cellular substrates of the MRI findings, while investigating the effects on the CNS following systemic inflammation. Lastly, since CPI can lead to a decrease in oxyhaemoglobin saturation (SaO_2) following the deterioration of pulmonary function, the current VBM findings (grey matter volume reduction in CPI-model rats) may encompass a hypoxic effect by given the observations of the reduction in some of the measured lung functions in CPI-model rats. Measuring SaO_2 and arterial partial pressure of oxygen (PaO_2) would be helpful for investigating the contribution of hypoxia to brain structural deficits after CPI. However, the present study lacks this data, since it focused on the neural effects of the inflammatory markers as a result of the systemic inflammation following pulmonary infection. Nonetheless, the quantified pulmonary functions, as well as the concentration of HIF-1α (a key transcriptional factor in hypoxia) in the present study could indirectly reflect the hypoxic levels to a certain extent (Kallio et al. 1999). Further, we considered the hypoxic effect by factoring out the pulmonary metrics and HIF-1α expression in a between-group comparison of voxel-based grey matter volume, as well as by correlating them to voxel-based grey matter volume. Results showed minimal changes in the brain grey matter volume reductions in CPI-model rats after adjusting for the pulmonary functions and HIF-1α levels, and none of them correlated with the voxel-based grey matter volume significantly. Although systemic hypoxia has been shown to cause grey matter volume reduction (e.g., Huang and Castillo, 2008), our CPI-model rats showed comparable lung compliance and FEV100/FVC to the control rats, as well as no significant increase in HIF-1α expression. This in turn indicated that the contribution of the hypoxic effect to

the current VBM findings was limited. Moreover, the current mediation analysis showed evidence for indirect effect of CPI on the changes of grey matter volume through histological changes and the enhanced levels of inflammatory markers, but not for pulmonary function parameters in mediating the changes in grey matter volume caused by CPI, which as a whole indicated that the potential hypoxia that resulted from the impaired lung functions did not mediate the brain consequence after CPI and provided compelling evidence supporting the intermediate effects of inflammatory processes in contributing to brain grey matter loss following CPI. Collectively, the present findings illustrated an important role of sustained pulmonary inflammation in the structural brain pathology of the diseases associated with CPI (such as COPD), while also establishing its general implications for other systemic inflammation diseases.

Conclusions

The present study demonstrated a neuroanatomical correlation pattern for various enhanced inflammatory markers and anxiety-like behaviours following CPI in rats. These findings not only elaborate the contribution of inflammatory markers to the brain structural pathology in chronic pulmonary diseases, and provide one possible explanation for the neurological and emotional symptoms presented in these patients, but also elucidate the general implications of chronic systemic inflammatory diseases on brain morphology. A combination of histological analysis may further help to understand the histopathology underpinning these MRI observations.

Funding:

This work was supported by National Science Foundation of China (Project NOs: 81171324; 81471630; 81472230).

Conflicts of interest:

The authors report no disclosures.

References

Ashburner, J., 2007. A fast diffeomorphic image registration algorithm. Neuroimage 38, 95-113.

Ashburner, J., Friston, K.J., 2000. Voxel-based morphometry-the methods. Neuroimage 11, 805-821.

Ashburner, J., Friston, K.J., 2005. Unified segmentation. Neuroimage 26, 839-851.

Banks, W.A., Farr, S.A., Morley, J.E., 2002. Entry of blood-borne cytokines into the central nervous system: effects on cognitive processes. Neuroimmunomodulation 10, 319-327.

Banks, W.A., 2005. Blood-brain barrier transport of cytokines: a mechanism for neuropathology. Current pharmaceutical design 11, 973-984.

Banks, W.A., 2015. The blood-brain barrier in neuroimmunology: tales of separation and assimilation. Brain, behavior, and immunity 44, 1-8.

Barnes, P.J., 2010. Chronic obstructive pulmonary disease: effects beyond the lungs. PLoS medicine 7, e1000220.

Biedermann, S.V., Fuss, J., Steinle, J., Auer, M.K., Dormann, C., Falfán-Melgoza, C., Ende, G., Gass, P., Weber-Fahr, W., 2016. The hippocampus and exercise: histological correlates of MR-detected volume changes. Brain Structure and Function 221, 1353-1363.

Brydon, L., Harrison, N.A., Walker, C., Steptoe, A., Critchley, H.D., 2008. Peripheral inflammation is associated with altered substantia nigra activity and psychomotor slowing in humans. Biological psychiatry 63, 1022-1029.

Capuron, L., Miller, A.H., 2004. Cytokines and psychopathology: lessons from interferon-α. Biological psychiatry 56, 819-824.

Cavaillon, J.-M., 2001. Pro-versus anti-inflammatory cytokines: myth or reality. CELLULAR AND MOLECULAR BIOLOGY-PARIS-WEGMANN- 47, 695-702.

Chevaleyre, V., Piskorowski, R.A., 2016. Hippocampal area CA2: an overlooked but promising therapeutic target. Trends in molecular medicine 22, 645-655.

Chen J, Lin I T, Zhang H, et al. 2016. Reduced cortical thickness, surface area in patients with chronic obstructive pulmonary disease: a surface-based morphometry and neuropsychological study. Brain imaging and behavior 10, 464-476.

Chen J, Zhang J, Liu X, et al. 2017. Abnormal subcortical nuclei shapes in patients with type 2 diabetes mellitus. European radiology 27, 4247-4256.

Crumeyrolle-Arias, M., Jaglin, M., Bruneau, A., Vancassel, S., Cardona, A., Daugé, V., Naudon, L., Rabot, S., 2014. Absence of the gut microbiota enhances anxiety-like behavior and neuroendocrine response to acute stress in rats. Psychoneuroendocrinology 42, 207-217.

Dantzer, R., Konsman, J.-P., Bluthé, R.-M., Kelley, K.W., 2000. Neural and humoral pathways of communication from the immune system to the brain: parallel or convergent? Autonomic Neuroscience: Basic and Clinical 85, 60-65.

Dantzer R, Bluthe RM, Castanon N, Kelly KW, Konsman J-P, Laye S, et al. 2007. Cytokines, sickness behavior, and depression. In: Ader R, editor. Psychoneuroimmunology, 4th ed. New York: Elsevier, 281–318.

Dantzer, R., O'Connor, J. C., Freund, G. G., Johnson, R. W., & Kelley, K. W., 2008. From inflammation to sickness and depression: when the immune system subjugates the brain. Nature reviews neuroscience, 9(1), 46.

Dinarello, C.A., 2000. Proinflammatory cytokines. Chest 118, 503-508.

Dodd J W, Chung A W, van den Broek M D, et al. 2012. Brain structure and function in chronic obstructive pulmonary disease: a multimodal cranial magnetic resonance imaging study[J]. American journal of respiratory and critical care medicine 186, 240-245.

Eisenberger, N.I., Berkman, E.T., Inagaki, T.K., Rameson, L.T., Mashal, N.M., Irwin, M.R., 2010. Inflammation-induced anhedonia: endotoxin reduces ventral striatum responses to reward. Biological psychiatry 68, 748-754.

Ek, M., Kurosawa, M., Lundeberg, T., Ericsson, A., 1998. Activation of vagal afferents after intravenous injection of interleukin-1β: role of endogenous prostaglandins. Journal of Neuroscience, 18(22), 9471-9479.

Frede, S., Stockmann, C., Freitag, P., Fandrey, J., 2006. Bacterial lipopolysaccharide induces HIF-1 activation in human monocytes via p44/42 MAPK and NF-κB. Biochemical Journal 396, 517-527.

Gadient, R., Otten, U., 1994. Expression of interleukin-6 (IL-6) and interleukin-6 receptor (IL-6R) mRNAs in rat brain during postnatal development. Brain research 637, 10-14.

Gu, Y., Vorburger, R., Scarmeas, N., Luchsinger, J.A., Manly, J.J., Schupf, N., Mayeux, R., Brickman, A.M.,

2017. Circulating inflammatory biomarkers in relation to brain structural measurements in a non-demented elderly population. Brain, behavior, and immunity 65, 150-160.

Guevara E, Pierre W C, Tessier C, et al. 2017. Altered Functional Connectivity Following an Inflammatory White Matter Injury in the Newborn Rat: A High Spatial and Temporal Resolution Intrinsic Optical Imaging Study. Frontiers in neuroscience11, 358.

Harrison, N.A., Brydon, L., Walker, C., Gray, M.A., Steptoe, A., Critchley, H.D., 2009. Inflammation causes mood changes through alterations in subgenual cingulate activity and mesolimbic connectivity. Biological psychiatry 66, 407-414.

Hayes, A.F., 2018. Introduction to mediation, moderation, and conditional process analysis: A regression-based approach (2nd Edition). New York: Guilford Press.

Higashida, T., Kreipke, C.W., Rafols, J.A., Peng, C., Schafer, S., Schafer, P., Ding, J.Y., Dornbos III, D., Li, X., Guthikonda, M., 2011. The role of hypoxia-inducible factor-1α, aquaporin-4, and matrix metalloproteinase-9 in blood-brain barrier disruption and brain edema after traumatic brain injury. Journal of neurosurgery 114, 92-101.

Hjerrild S, Renvillard S G, Leutscher P, et al. 2016. Reduced cerebral cortical thickness in Non-cirrhotic patients with hepatitis C. Metabolic brain disease, 31, 311-319.

Hu, J., Ferreira, A., Van Eldik, L.J., 1997. S100β induces neuronal cell death through nitric oxide release from astrocytes. Journal of neurochemistry 69, 2294-2301.

Hu, J., Van Eldik, L.J., 1999. Glial-derived proteins activate cultured astrocytes and enhance beta amyloid-induced glial activation. Brain research 842, 46-54.

Huang, B. Y., & Castillo, M. 2008. Hypoxic-ischemic brain injury:imaging findings from birth to adulthood. Radiographics 28,417–439.

Hunt, D., Coffin, R., Prinjha, R., Campbell, G., Anderson, P., 2003. Nogo-A expression in the intact and injured nervous system. Molecular and Cellular Neuroscience 24, 1083-1102.

Hunter, C.A., Jennings, F.W., Kennedy, P., Murray, M., 1992. Astrocyte activation correlates with cytokine production in central nervous system of Trypanosoma brucei brucei-infected mice. Laboratory investigation; a journal of technical methods and pathology 67, 635-642.

Hynninen, K.M.J., Breitve, M.H., Wiborg, A.B., Pallesen, S., Nordhus, I.H., 2005. Psychological characteristics of patients with chronic obstructive pulmonary disease: a review. Journal of psychosomatic research 59, 429-443.

Jack Jr, C., Twomey, C., Zinsmeister, A.R., Sharbrough, F., Petersen, R.C., Cascino, G.D., 1989. Anterior temporal lobes and hippocampal formations: normative volumetric measurements from MR images in young adults. Radiology 172, 549-554.

Jaeger, L.B., Dohgu, S., Sultana, R., Lynch, J.L., Owen, J.B., Erickson, M.A., Shah, G.N., Price, T.O., Fleegal-Demotta, M.A., Butterfiled, D.A., 2009. Lipopolysaccharide alters the blood–brain barrier transport of amyloid β protein: a mechanism for inflammation in the progression of Alzheimer's disease. Brain, behavior, and immunity 23, 507-517.

Katon, W., Lozano, P., Russo, J., McCauley, E., Richardson, L., Bush, T., 2007. The prevalence of DSM-IV anxiety and depressive disorders in youth with asthma compared with controls. Journal of Adolescent Health 41, 455-463.

Kallio P. J., Wilson W. J., O'Brien S., Makino Y. and Poellinger L. 1999. Regulation of the hypoxia-inducible transcription factor 1a by the ubiquitin-proteasome pathway. J. Biol. Chem. 274, 6519–6525

Kesler, S., Janelsins, M., Koovakkattu, D., Palesh, O., Mustian, K., Morrow, G., Dhabhar, F.S., 2013. Reduced hippocampal volume and verbal memory performance associated with interleukin-6 and tumor necrosis factor-alpha levels in chemotherapy-treated breast cancer survivors. Brain, behavior, and immunity 30, S109-S116.

Khan, M., Khan, H., Singh, I., Singh, A.K., 2017. Hypoxia inducible factor-1 alpha stabilization for regenerative therapy in traumatic brain injury. Neural regeneration research 12, 696.

Kim, K.S., Wass, C., Cross, A., Opal, S., 1992. Modulation of blood-brain barrier permeability by tumor necrosis factor and antibody to tumor necrosis factor in the rat. Lymphokine and cytokine research 11, 293-298.

Kjonigsen L J, Lillehaug S, Bjaalie J G, et al. 2015. Waxholm Space atlas of the rat brain hippocampal region: three-dimensional delineations based on magnetic resonance and diffusion tensor imaging. Neuroimage108, 441-449.

Konsman, J.P., Parnet, P., Dantzer, R., 2002. Cytokine-induced sickness behaviour: mechanisms and implications. Trends in neurosciences, 25(3), 154-159.

Korfias, S., Stranjalis, G., Papadimitriou, A., Psachoulia, C., Daskalakis, G., Antsaklis, A., Sakas, D., 2006. Serum S-100B protein as a biochemical marker of brain injury: a review of current concepts. Current medicinal chemistry 13, 3719-3731.

Lam, A.G., Koppal, T., Akama, K.T., Guo, L., Craft, J.M., Samy, B., Schavocky, J.P., Watterson, D.M., Van Eldik, L.J., 2001. Mechanism of glial activation by S100B: involvement of the transcription factor NFκB. Neurobiology of aging 22, 765-772.

Li, Q., Cheung, C., Wei, R., Hui, E.S., Feldon, J., Meyer, U., Chung, S., Chua, S.E., Sham, P.C., Wu, E.X., 2009. Prenatal immune challenge is an environmental risk factor for brain and behavior change relevant to schizophrenia: evidence from MRI in a mouse model. PloS one 4, e6354.

Maier, S.F., Watkins, L.R., 1998. Cytokines for psychologists: implications of bidirectional immune-to-brain communication for understanding behavior, mood, and cognition. Psychological review 105, 83.

Marsland, A.L., Gianaros, P.J., Abramowitch, S.M., Manuck, S.B., Hariri, A.R., 2008. Interleukin-6 covaries inversely with hippocampal grey matter volume in middle-aged adults. Biological psychiatry 64, 484-490.

Marsland, A.L., Gianaros, P.J., Kuan, D.C.-H., Sheu, L.K., Krajina, K., Manuck, S.B., 2015. Brain morphology links systemic inflammation to cognitive function in midlife adults. Brain, behavior, and immunity 48, 195-204.

May, A., Gaser, C., 2006. Magnetic resonance-based morphometry: a window into structural plasticity of the brain. Current opinion in neurology 19, 407-411.

Miklos S, Mueller G, Chang Y, et al. 2008. Pulmonary function changes in experimental graft-versus-host disease of the lung. Biology of Blood and Marrow Transplantation14, 1004-1016.

Nie, B., Chen, K., Zhao, S., Liu, J., Gu, X., Yao, Q., Hui, J., Zhang, Z., Teng, G., Zhao, C., 2013. A rat brain MRI template with digital stereotaxic atlas of fine anatomical delineations in paxinos space and its automated application in voxel-wise analysis. Human brain mapping 34, 1306-1318.

Opal, S.M., Depalo, V.A., 2000. Anti-inflammatory cytokines. Chest 117, 1162-1172.

Oyarzabal, E.A., 2016. The role of astrocytes in response to stimulation with the microbial endotoxin lipopolysaccharide. Doctoral dissertation, The University of North Carolina at Chapel Hill.

Papp, E.A., Leergaard, T.B., Calabrese, E., Johnson, G.A., Bjaalie, J.G., 2014. Waxholm Space atlas of the Sprague Dawley rat brain. Neuroimage 97, 374-386.

Parsadaniantz, S. M., Lebeau, A., Duval, P., Grimaldi, B., Terlain, B., Kerdelhue, B., 2000. Effects of the Inhibition of Cyclo-Oxygenase 1 or 2 or 5-Lipoxygenase on the Activation of the Hypothalamic-Pituitary-Adrenal Axis Induced by Interleukin-1β in the Male Rat. Journal of neuroendocrinology,

12(8), 766-773.

Paxinos, G., Watson, C., 2014. Paxino's and Watson's the Rat Brain in Stereotaxic Coordinates Seventh edition. Elsevier/AP, Academic Press is an imprint of Elsevier, Amsterdam; Boston.

Pham D L, Prince J L. 1999. An adaptive fuzzy C-means algorithm for image segmentation in the presence of intensity inhomogeneities. Pattern recognition letters 20, 57-68.

Perry, V.H., Cunningham, C., Holmes, C., 2007. Systemic infections and inflammation affect chronic neurodegeneration. Nature Reviews Immunology 7, 161.

Pessoa, L., 2017. A network model of the emotional brain. Trends in cognitive sciences 21, 357-371.

Prut, L., Belzung, C., 2003. The open field as a paradigm to measure the effects of drugs on anxiety-like behaviors: a review. European journal of pharmacology 463, 3-33.

Quan, N., Whiteside, M., & Herkenham, M., (1998). Time course and localization patterns of interleukin-1β messenger RNA expression in brain and pituitary after peripheral administration of lipopolysaccharide. Neuroscience, 83(1), 281-293.

Raghavendra, V., Tanga, F.Y., DeLeo, J.A., 2004. Complete Freunds adjuvant-induced peripheral inflammation evokes glial activation and proinflammatory cytokine expression in the CNS. European Journal of Neuroscience 20, 467-473.

Ramilo, O., Saez-Llorens, X., Mertsola, J., Jafari, H., Olsen, K., Hansen, E., Yoshinaga, M., Ohkawara, S., Nariuchi, H., McCracken, G., 1990. Tumor necrosis factor alpha/cachectin and interleukin 1 beta initiate meningeal inflammation. Journal of Experimental Medicine 172, 497-507.

Reichenberg, A., Yirmiya, R., Schuld, A., Kraus, T., Haack, M., Morag, A., Pollmächer, T., 2001. Cytokine-associated emotional and cognitive disturbances in humans. Archives of general psychiatry 58, 445-452.

Rius, J., Guma, M., Schachtrup, C., Akassoglou, K., Zinkernagel, A.S., Nizet, V., Johnson, R.S., Haddad, G.G., Karin, M., 2008. NF-κB links innate immunity to the hypoxic response through transcriptional regulation of HIF-1α. Nature 453, 807.

Rivest, S., 2001. How circulating cytokines trigger the neural circuits that control the hypothalamic–pituitary–adrenal axis. Psychoneuroendocrinology 26, 761-788.

Rothermundt, M., Peters, M., Prehn, J.H., Arolt, V., 2003. S100B in brain damage and neurodegeneration. Microscopy research and technique 60, 614-632.

Sastre, M., Walter, J., Gentleman, S.M., 2008. Interactions between APP secretases and inflammatory

mediators. Journal of neuroinflammation 5, 25.

Semmler, A., Okulla, T., Sastre, M., Dumitrescu-Ozimek, L., Heneka, M.T., 2005. Systemic inflammation induces apoptosis with variable vulnerability of different brain regions. Journal of chemical neuroanatomy 30, 144-157.

Shao, B., Teng, L., Peng, Y., Chen, H., He, X., Duan, H., Yang, P., Chen, Y., 2017. Expression changes and significance of neurite outgrowth inhibitor A (Nogo-A), glial fibrillary acidic protein and insulin-like growth factor-1 in rat brain tissues after craniocerebral injury. Biomedical Research 28.

Smith, S.M., Jenkinson, M., Woolrich, M.W., Beckmann, C.F., Behrens, T.E., Johansen-Berg, H., Bannister, P.R., De Luca, M., Drobnjak, I., Flitney, D.E., 2004. Advances in functional and structural MR image analysis and implementation as FSL. Neuroimage 23, S208-S219.

Stolk, J., Rudolphus, A., Davies, P., Osinga, D., Dijkman, J.H., Agarwal, L., Keenan, K.P., Fletcher, D., Kramps, J.A., 1992. Induction of emphysema and bronchial mucus cell hyperplasia by intratracheal instillation of lipopolysaccharide in the hamster. The Journal of pathology 167, 349-356.

Tancredi, V., D'Antuono, M., Cafè, C., Giovedì, S., Buè, M.C., D'Arcangelo, G., Onofri, F., Benfenati, F., 2000. The inhibitory effects of interleukin-6 on synaptic plasticity in the rat hippocampus are associated with an inhibition of mitogen-activated protein kinase ERK. Journal of neurochemistry 75, 634-643.

Tambalo S, Peruzzotti-Jametti L, Rigolio R, et al. 2015. Functional magnetic resonance imaging of rats with experimental autoimmune encephalomyelitis reveals brain cortex remodeling. Journal of Neuroscience, 35, 10088-10100.

Vernooy, J.H., Küçükaycan, M., Jacobs, J.A., Chavannes, N.H., Buurman, W.A., Dentener, M.A., Wouters, E.F., 2002b. Local and systemic inflammation in patients with chronic obstructive pulmonary disease: soluble tumor necrosis factor receptors are increased in sputum. American journal of respiratory and critical care medicine 166, 1218-1224.

Vitkovic, L., Konsman, J., Bockaert, J., Dantzer, R., Homburger, V., Jacque, C., 2000. Cytokine signals propagate through the brain. Molecular psychiatry 5, 604.

Von Leupoldt, A., Brassen, S., Baumann, H.J., Klose, H., Büchel, C., 2011. Structural brain changes related to disease duration in patients with asthma. PloS one 6, e23739.

Walsh, R.N., Cummins, R.A., 1976. The open-field test: a critical review. Psychological bulletin 83, 482.

Wartolowska K, Hough M G, Jenkinson M, et al. 2012. Structural changes of the brain in rheumatoid arthritis. Arthritis & Rheumatology64, 371-379.

Wright, C., Strike, P., Brydon, L., Steptoe, A., 2005. Acute inflammation and negative mood: mediation by cytokine activation. Brain, behavior, and immunity 19, 345-350.

Yang, S.H., Gangidine, M., Pritts, T.A., Goodman, M.D., Lentsch, A.B., 2013. Interleukin 6 mediates neuroinflammation and motor coordination deficits after mild traumatic brain injury and brief hypoxia in mice. Shock (Augusta, Ga.) 40, 471.

Yarkoni, T., 2009. Big correlations in little studies: Inflated fMRI correlations reflect low statistical power—Commentary on Vul et al., 2009. Perspectives on Psychological Science, 4(3), 294-298.

Yeh, S.H., Ou, L.C., Gean, P.W., Hung, J.J., Chang, W.C., 2011. Selective Inhibition of Early-but Not Late-Expressed HIF-1α Is Neuroprotective in Rats after Focal Ischemic Brain Damage. Brain Pathology 21, 249-262.

Zatorre, R.J., Fields, R.D., Johansen-Berg, H., 2012. Plasticity in gray and white: neuroimaging changes in brain structure during learning. Nature neuroscience 15, 528.

Zhang, H., Sachdev, P.S., Wen, W., Crawford, J.D., Brodaty, H., Baune, B.T., Kochan, N.A., Slavin, M.J., Reppermund, S., Kang, K., 2016a. The relationship between inflammatory markers and voxel-based gray matter volumes in nondemented older adults. Neurobiology of aging37, 138-146.

Zhang Z, Wang Y, Shen Z, et al. 2016b. The neurochemical and microstructural changes in the brain of systemic lupus erythematosus patients: A multimodal MRI study. Scientific reports, 6, 19026.

Zikou A K, Kosmidou M, Astrakas L G, et al. 2014. Brain involvement in patients with inflammatory bowel disease: a voxel-based morphometry and diffusion tensor imaging study. European radiology 24, 2499-2506.

Figure Legends

Figure. 1. Two flow chartsdemonstrate the whole experiment (A) and the computational processing of the structural MRI data which then derives the voxel-based grey matter measurement (B) in the present study.

Figure. 2. Pearson correlations between the 12 measured inflammatory markers plus HIF-1α in controls and CPI-model rats. Different correlation patterns were noticed between the two

groups. Significant correlations were marked with asterisks (*p < 0.05, **p < 0.01). Correlation coefficients are color-coded, yellow to red indicates the strength of positive correlation while cyan to blue indicates the negative correlation.

Figure. 3. Significant between-group differences in voxel-based grey matter volume. A widespread grey matter volume reduction was revealed in CPI-models rats. Strength of statistical significance is color-coded with lavender to red indicating FWE-corrected P values from 0.01 to 0.001. Blue refers to those grey matter volume reduction areas at a FWE-corrected p range of 0.05-0.01, presenting how the grey matter volume reduction is extended to neighbouring brain regions after lower the threshold. Slice location in relation to bregma (mm). Thal, thalamus; Hypo-Thal, hypo-thalamus; Amy, amygdala; SN, substantia nigra; LGP, lateral globus pallidus; CPu, caudate putamen; RS, retrosplenial cortex; M1/M2, motor cortex; S1, somatosensory cortex; LSI, lateral septal nucleus; Ins, insular cortex; Cg, cingulate cortex; AuC, auditory cortex; VC, visual cortex; SC, superior colliculus; PER, perirhinal cortex; TeA, temporal association cortex; Ect, ectorhinal cortex; Ent, entorhinal cortex.

Figure. 4. Results of the individual general linear models (GLMs) presenting the association between each inflammatory maker and voxel-based grey matter volume. A. Anatomical regions revealed in all of the GLM analyses, which were taken from the Waxholm Space MRI atlas. Name for each region was illustrated by 14 color-blocks in the right side. B. Brain MRI sections showing areas that were significantly negatively correlated with the inflammatory marker-levels after TFCE estimation with a FWE-corrected threshold of p < 0.05. Strength of the statistical significance was color-coded at the bottom of these MRI brain slices. Red lines outline the brain regions with significantly decreased voxel-based grey matter volumes in CPI-model rats. Slice location in relation to bregma (mm). C. Heat map demonstrating correlation coefficients of those significantly correlated regions for the 8 inflammatory markers. The significant coefficients were color-coded from light green to dark blue to indicate the correlation strength. Non-significant correlations were shown in white. Thal, thalamus; Hypo-Thal, hypo-thalamus; SN, substantia nigra; LGP, lateral globus pallidus; CPu, caudate putamen; LSI, lateral septal nucleus; Ins, insular cortex; Cg, cingulate cortex; SC, superior colliculus; PER, perirhinal cortex.

Figure. 5. Region-of-interest (ROI)-based correlation analysis for testing the relationship between grey matter volume and behavior metrics (open field test) which showed no significance in

whole brain voxel-wise correlation analysis. A. Sphere ROIs were created after consultation with the Paxinos' stereotactic rat brain atlas with radiuses of 0.4 mm, and the mean grey matter volumes extracted within these ROIs were used for ROI-based correlation analysis. B. Scatter plots are shown of the averaged grey matter volumes within the ROIs in positive correlations with the open field activities of number of grooming, number of rearing and the crossing counts. Three regression lines were shown in the scatter plots [overall (black), control (blue), CPI-model (red)] with the correlation values stated within the figures. * $p < 0.05$. M1, primary motor cortex; S1, primary somatosensory cortex; Amy, amygdala; RS, retrosplenial cortex; Ins, insular cortex; VC, visual cortex; Ect, ectorhinal cortex;TeA, temporal association cortex; AuC, auditory cortex.

Figure. 6. Nissl staining and immunofluorescence results from the focused histological analysis. A.From left to right showing 1). Grey matter volume reduction area in CPI-model rats which derived from the whole brain voxel-based between-group comparison; 2). ROIs selected for histological analysis on volumetric MRI slice which were color-coded at the right extreme. MRI slice location in relation to bregma (mm); 3). Frames outlined on the anatomical brain section according to the MRI ROIs. B. Expressions of S100β and Nogo-A proteins, as well as the Nissl stained neuronal cells within the selected brain regions. C. Bar charts of the between-group differences of the fluorescence intensity per area (Integrated intensity/Area) and relative cell area indices. Values of these two indices were derived from the ImageJ software based on the immunofluorescence and Nissl images in B. Amy, amygdala; RS, retrosplenial cortex; Ins, insular cortex; Hypo-Thal, hypo-thalamus.

Figure. 7 Between-group comparison of whole brain voxel-wise grey matter volume after controlling for A. HIF-1α level; B. FEV50/FVC; and C. FRC. Strength of the statistical significance is color-coded. Lavender to red indicates TFCE FWE-corrected p from 0.01 to 0.001, and blue indicates the brain areas survived after increase the TFCE FWE-corrected p value from 0.01 to 0.05. FEV, forced expiratory volume; FVC, forced vital capacity; FRC, functional residual capacity.

Supplementary figure. 1 Scatters showing the significant correlations between the 8 inflammatory markers and brain grey matter volumes in multiple regions consecutively for IL-1β (A), IL-6 (B), TNF-α (C), IL-10 (D), IL-8 (E), CC16 (F), MMP-9 (G), and CRP (H). Three regression lines were shown in the provided scatter plots [overall (black), control (blue), CPI-model (red)] with the correlation values stated within the figures. ** $p < 0.01$, * $p < 0.05$ or those correlations with

p < 0.1 but approached large effect sizes. Thal, thalamus; Hypo-Thal, hypo-thalamus; Amy, amygdala; SN, substantia nigra; LGP, lateral globus pallidus; CPu, caudate putamen; RS, retrosplenial cortex; M1, motor cortex; S1, somatosensory cortex; LSI, lateral septal nucleus; Ins, insular cortex; Cg, cingulate cortex; AuC, auditory cortex; VC, visual cortex; SC, superior colliculus; PER, perirhinal cortex; TeA, temporal association cortex; Ect, ectorhinal cortex.

Supplementary figure. 2 Scatters showing the significant correlations between histological metrics (fluorescence intensity per area for S100β and Nogo-A, and relative cell area for Nissl staining) and the corresponding MRI derived grey matter volumes in CA3, amygdala and hypo-thalamus.

Supplementary figure. 3 Diagram shows the primary mediation model in testing the possible mediators of histological metrics, i.e., the indirect effect (a*b) of histological changes in mediating the experimental condition (chronic pulmonary inflammation; CPI) on the changes in brain grey matter volume. An ordinary least squares path analysis was employed. The a-path refers to the experimental effect on the possible mediator, while the b-bath tests for the effect of mediator in predicting the changes in grey matter volume after controlling for c'-path, i.e., the direct effect of CPI on grey matter volume changes.

Table 1. Inflammatory markers, behavior measures and global MRI metrics of the CPI-model rats and the control rats

Characteristics	CPI-model group (N=20)	Control group (N=25)	*P*
Inflammatory markers			
Pro-inflammatory			
IL-1β (ng/L)	27.39±0.95	25.08±1.63	**<0.001***
IL-6 (pg/ml)	82.36±3.18	76.11±4.37	**<0.001***
TNF-α (ng/L)	235.02±6.37	215.06±14.35	**<0.001***
IFN-γ (pg/ml)	1371.81±32.89	1340.34±37.63	**0.012**
GM-CSF (ng/L) ***Anti-inflammatory***	182.92±6.44	178.53±10.41	0.137
IL-10 (ng/L)	59.67±2.38	57.44±2.47	**0.009**
TGF-β (pg/ml)	190.11±7.10	186.74±9.05	0.221
Chemokines			
IL-8 (ng/L)	314.91±10.78	293.02±20.18	**<0.001***
CXCL2 (ng/L)	69.03±2.54	66.40±2.50	**0.004**
CC16 (ng/L)	330.01±10.92	309.22±13.35	**<0.001***
Others			
CRP (μg/L)	4.94±0.18	4.64±0.21	**<0.001***
MMP-9 (μg/L)	54.34±1.95	49.61±2.83	**<0.001***
HIF-1α (ng/L)	50.61±1.92	49.21±2.44	0.064
Behavior measures (open field)			
Number of center entries	1 (0-7)	0 (0-3)	0.146
Crossing counts	27.08±17.76	40.87±16.01	**0.023**
Number of defecation	0 (0-5)	1 (0-5)	0.244
Number of grooming	2.31±1.80	4.83±3.30	**0.016**
Number of rearing	5.31±4.52	9.96±4.94	**0.008**
Global metrics of the structural MRI (ml)			
Total GM	1.777±0.101	1.891±0.093	**<0.001***
Total WM	0.386±0.045	0.362±0.058	0.144
Total CSF	0.253±0.048	0.191±0.053	**<0.001***
ICV	2.416±0.122	2.445±0.087	0.356

P-values in bold indicate a significance of $P < 0.05$, *indicates the between-group comparisons survived after Bonferroni correction. These p-values were determined by two sample t-tests except for the measurements of number of defecation and number of center entries, which were identified by two sample Mann–Whitney *U* test according to their data distributions. Except for number of center entries and number of defecation which are shown as median (range), data are in mean ± standard deviation.

Highlights:

- Chronic pulmonary inflammation results in decreased brain grey matter volume (GMV).
- Elevated circulating inflammatory markers (IMs) correlate to brain GMV reduction.
- The various IMs present differential neuroanatomical correlation patterns.
- Lower GMVs in IM-related brain regions are associated with anxiety-like behaviors.
- The *in-vivo* MRI findings are validated by postmortem histological measurements.